ANNALI DI GEOFISICA, VOL. XL, N. 4, August 1997

The ionosphere and radio interferometry

Titus A. Th. Spoelstra
Netherlands Foundation for Research in Astronomy, Dwingeloo, The Netherlands

Abstract
This paper reviews the effects of the ionosphere on radio astronomical observations, what we can learn about the ionosphere from radio interferometry, and a procedure to correct for these effects. This study analyzes the results obtained from observations of celestial point sources with the Westerbork Synthesis Radio Telescope, WSRT, in the Netherlands from the period 1970-1991. The main conclusions are: 1) Although seasonal effects are clear, the occurrence and «strength» of ionospheric irregularities show no dependence on solar activity. 2) Assuming that the frequency of occurrence of ionospheric disturbances in Spring and Autumn are similar, the «ionospheric» Winter starts on day 348 ± 3 and all seasons last for three months. 3) Travelling ionospheric disturbances, TIDs, occur most frequently during daytime in Winter periods. 4) The propagation parameters of these travelling ionospheric irregularities and their periods indicate that these belong mainly to the class of medium scale TIDs. 5) Radio interferometry is a powerful tool to locate irregularities causing scintillation and to determine their dimensions. 6) The occurrence of non-periodic irregularities is, however, not a function of time of day. 7) The daily variation in the amplitude and frequency of occurrence of the TIDs suggest that the generation of gravity waves may be caused by winds and tides in the lower thermosphere/mesosphere. On the basis of the available data, a definition of a «disturbance measure» indicating to what extent the ionosphere is «quiet» is proposed. Procedures to correct for ionospheric effects and an evaluation of the different methods to obtain information on the ionospheric electron content are reviewed in sections 8 and 9, respectively.

Key words *ionosphere – radio interferometry*

1. Introduction

The characteristics of radio waves propagating through a volume of space filled by a medium are affected depending on the medium and its nature. The ionosphere and troposphere cause the most significant modifications of these wave characteristics for earth based reception techniques. These modifications may be noticeable as *e.g.*, refraction, reflection, scintillation, emission and/or absorption effects. These effects are observed as modifications of the signal intensity (and polarization characteristics) and the signal path (or signal delay).

The magnitude of the observed effects depends not only on the nature of the medium but also on the frequency used in the experiment, the characteristics of the receiving equipment (*e.g.*, beamwidth, bandwidth, integration time, number of antennae or elements and how their output is correlated), detection method (*e.g.*, timescale of the direction and/or frequency changes – if any, sample interval), source characteristics (*e.g.*, position, frequency, polarization), time (*e.g.*, seasons, solar activity, geomagnetic activity).

In this review we address the question of the influence of the ionosphere in radio astronomical observations. This question can be ap-

Mailing address: Dr. Titus A. Th. Spoelstra, Netherlands Foundation for Research in Astronomy, P.O. Box 2, 7990 AA Dwingeloo, The Netherlands; e-mail: spoelstra@nfra.nl

proached from the interest of aeronomy and as a problem which affects the quality of radio astronomical measurement results. Attention will be paid to both aspects: the ionosphere as an object of study and the ionosphere as a nuisance.

In radio astronomy, at wavelengths of decimeters or longer, the ionosphere usually affects the observations as a refraction effect. This refraction effect is manifest as a position shift of the observed celestial radio source and a change of its structure, and as a Faraday rotation of the polarization angle of emission from a polarized radio source. (Faraday rotation is caused by differential refraction for left and right circularly polarized signals). It is well-known that the ionospheric electron density shows spatial and temporal variations at many different spatial and time scales. Significant deviations from the condition of the «quiet» ionosphere are frequently called «disturbances» (sections 5 and 7).

The fundamental phenomenon of a refraction effect is a delay error. In radio interferometry it translates into a phase error (section 4). Ionospheric refraction is a significant effect for connected element interferometry at frequencies up to about 2 GHz. Of course there is a smooth transition from refraction into diffraction. Diffraction occurs when the angular scale of ionospheric irregularities is less than the beamwidth of an interferometer element. In that case ionospheric irregularities above the different interferometer elements may be uncorrelated. This effect is then visible in the observations as scintillations in interferometer phase and/or amplitude. Although in general the observing frequencies used in Very Long Baseline Interferometry, VLBI, are higher than 2 GHz, the long baselines involved imply that this technique is also sensitive to ionospheric effects at these frequencies.

It is evident that radio interferometric «observables» contain information about the medium through which the signal propagates, *i.e.*, the ionospheric total electron content and its variations with time and geographical coordinates. This information combined with results from other techniques to determine ionospheric parameters extends our knowledge of ionospheric «climate».

One wants to avoid ionospheric disturbances as much as possible and if possible correct for ionospheric effects on wave propagation: the «undisturbed» ionosphere is already difficult enough. Radio astronomy is not different from other applications using transionospheric radio signals. To achieve this goal, it is relevant to know the conditions under which these disturbances can be expected. Input for this knowledge should be the climatology of ionospheric irregularities.

Section 2 gives necessary instrumental background for radio interferometry. In section 3 we summarize the relevant propagation effects on the measured signals. A specific implementation of radio interferometry, the Westerbork Synthesis Radio Telescope, WSRT, and its data base are described in section 4. A climatology of ionospheric irregularities derived from WSRT observations is discussed in section 5. The effect of scintillation on radio interferometric measurements is reviewed in section 6 for weak and intense scintillation. It turns out that radio interferometry is a powerful tool to study ionospheric irregularities causing scintillation of radio waves.

Several classes of ionospheric irregularities are interpreted in terms of acoustic-gravity waves travelling through the ionosphere. Medium scale travelling ionospheric disturbances, TIDs, have typical periods of 10-30 min, horizontal wavelengths between 100 and 300 km and speeds of 100-300 m/s. Large scale TIDs have longer periods, horizontal wavelengths up to a few thousand kilometers and speeds of 300-1000 m/s. Small scale TIDs with speeds up to 1000 m/s but periods less than a few minutes are acoustic waves.

The knowledge of the kinematic parameters of travelling ionospheric disturbances is an essential basis for their physical understanding and investigation of their possible excitation mechanisms. Among the different parameters of the TIDs the propagation speeds and directions in particular are important. This aspect of ionospheric irregularities is also summarized in section 5.

A definition of «quiet» and «disturbed» and the practical use of this concept are outlined in section 7.

Table I. Symbols for quantities used.

Az	= azimuth
$\vec{B}$	= interferometer baseline
$\vec{B}_0$	= true interferometer baseline: *i.e.*, when refraction is absent
b	= speed of travelling ionospheric irregularities
c	= speed of light
$D_{\Delta\phi}(\vec{r}-\vec{r}\,')$	= optical path structure function
d	= total effective thickness of the ionosphere $\left(d=\frac{2}{3}(y_m+y_m')\right)$
e	= charge of electron
$F(\nu)$	= frequency passband characteristics
f	= fringe rate
f_H	= geomagnetic gyrofrequency ($f_H = \lvert eB/(2\pi m_e)\rvert$)
f_0	= critical frequency
$f_0F_2(t)$	= critical frequency of F_2-layer at time t
$G(\vec{r}-\vec{r}_0)$	= primary antenna power pattern
H	= field strength of the geomagnetic field
$H(\vec{\kappa}, \nu, z)$	= spatial amplitude filter function,
	defined as $H(\vec{\kappa}, \nu, z)=\left[1-\frac{2k}{\kappa_p^2}L\sin\left(\frac{\kappa_p^2 L}{2k}\right)\cos\left(\frac{\kappa_p^2}{k}\left(z-\frac{L}{2}\right)\right)\right]$
$I(\vec{r}-\vec{r}_0)$	= interferometer response to an extended radio source
$I(\vec{B}, \vec{\kappa}, \nu)$	= spatial interferometer amplitude filter function,
	defined as $I(\vec{B}, \vec{\kappa}, \nu)=\gamma^2[1+\cos\vec{\kappa}_p\cdot\vec{B}]$
j	= $\sqrt{(-1)}$
k	= wave number of radio signal
k_0	= zenith angle, angle between the ray and the local vertical, at ionospheric height (assumed value: 350 km)
k_{0m}	= zenith angle, angle between the ray and the local vertical, at height of maximum electron density
L	= thickness of region of random irregular electron density structure
m_e	= mass of electron
N	= electron density ($N = 2\pi f_0^2 m_e \varepsilon/e^2$)
$N(\vec{r})$	= electron density distribution
N_e	= columnar electron content
$n(\vec{s}, \nu)$	= refractive index ($n(\vec{s}, \nu) = 1-X/(1+Y\cos\theta - jZ)$ if $\nu \lesssim 15$ MHz)
$P(\vec{\kappa}, \nu, z)$	= spatial phase filter function,
	defined as $P(\vec{\kappa}, \nu, z)=\left[1+\frac{2k}{\kappa_p^2 L}\sin\left(\frac{\kappa_p^2 L}{2k}\right)\cos\left(\frac{\kappa_p^2}{k}\left(z-\frac{L}{2}\right)\right)\right]$
p	= fraction of total electron content involved in density waves

Table I (*continued*).

$Q(\vec{B}, \vec{\kappa})$	= spatial interferometer phase filter function, defined as $Q(\vec{B}, \vec{\kappa}) = [1 - \cos \vec{\kappa}_p \cdot \vec{B}]$
R_e	= radius of the Earth
$R(\nu, \vec{r})$	= interferometer response
$\vec{r}$	= direction to celestial radio source
r_b	= radius of bottomside of F_2-region
r_e	= distance from Earth centre
r_{el}	= classical electron radius
r_m	= radius of the surface of maximum electron density
$\vec{r}_0$	= true direction to celestial radio source
r_t	= radius of topside of F_2-region
S_1	= phase scintillation index; S_1^2 mean square of phase fluctuations
S_4	= scintillation index, defined as $S_4^2 = \dfrac{<R(\nu, \vec{r})^2> - <R(\nu, \vec{r})>^2}{<R(\nu, \vec{r})>^2}$
S_ν	= flux of celestial radio source
$\vec{s}$	= ray path
TEC	= (vertical) total electron content; defined as $\text{TEC} = \dfrac{1}{\cos k_0} \int_s N(r)\, ds$
t	= time
$U(\vec{r}, \nu, z)$	= measured response of radio wave travelling through the ionosphere
$V(\vec{B})$	= visibility function
X	= component of ionospheric refraction index ($X = f_0^2/\nu^2$)
Y	= component of ionospheric refraction index ($Y = f_H/\nu$)
y, y'	= «semithickness» of regions above and below maximum density (a parabolic model for the electron density as a function of altitude was assumed)
Z	= component of ionospheric refraction index ($Z = \nu_c/(2\pi\nu)$)
z	= z-coordinate in (x, y, z) orthogonal coordinate system; z is usually perpendicular to the Earth's surface
z_i	= zenith angle in the ionospheric point
z_r	= zenith angle at the receiver
α	= right ascension
β_g	= geographical latitude
β_I	= 1/2 half-power-beamwidth of interferometer element I
$\Gamma(\vec{r}, \vec{r}', \nu, z)$	= coherence function
γ	= factor for the near field corrections
δ	= declination
Δf_a	= fringe rate errors due to atmospheric propagation effects
Δf_c	= fringe rate errors due to clock errors, the rotation of the Earth, etc.
Δf_{obs}	= observed fringe frequency
$\Delta\vec{r}$	= range error
Δt	= clock error
$\Delta\alpha$	= refraction angle (right ascension)

Table I (*continued*).

$\Delta\delta$	= refraction angle (declination)
$\Delta\delta_p$	= error in the declination of the baseline pole
$\Delta\delta_s$	= refraction angle (declination) – spherical component
$\Delta\delta_w$	= refraction angle (declination) – wedge component
$\Delta\nu$	= frequency bandwidth
$\Delta\phi$	= interferometer phase variation
$\Delta\phi_N$	= variation phase path NNSS signals due to refraction
$\Delta\psi$	= ionospheric Faraday rotation
$\Delta\tau$	= differential time delay over frequency band $\Delta\nu$
$\Delta\tau_a$	= atmospheric delay errors
$\Delta\tau_c$	= sum of effects of clock errors, of the rotation of the Earth, etc.
$\Delta\tau_0$	= observed time delay
ε	= dielectric constant
ε_0	= free space dielectric permittivity
$\varepsilon_1(\vec{r}, t)$	= dielectric permittivity in the ionosphere
η	= spectral index of power law spectrum
ζ	= distance from antenna to region of random irregular electron distribution
θ	= angle between wave normal and the direction of the magnetic field
κ_p	= wavenumher of fluctuations perpendicular to line of sight
λ	= observing wavelength
λ_E	= longitude to the east of the observer
λ_g	= longitude measured eastward from the observer
ν	= frequency of the electromagnetic wave
ν_c	= collision frequency
ν_{IF}	= IF frequency
ν_0	= local oscillator frequency
ϕ	= interferometer phase
ϕ_N	= phase path NNSS signals
ϕ_a	= latitude of the point at which the ray intersects the upper ionospheric boundary
Φ	= geographic latitude
Φ_0	= geographic latitude of the observer
$\Phi_{\Delta N}(\kappa_p, \kappa_z)$	= 3-dimensional spectrum of ionospheric electron density fluctuations
$\Phi_\phi(\vec{\kappa}_p)$	= power spectrum for the phase $\phi(\vec{r})$
ψ	= angle between the long axis of ionospheric irregularities and line of sight
ψ_{pol}	= polarization angle
$\Psi(\vec{r}, \nu, z)$	= distribution function of scintillation induced perturbations
$\sigma_1(\vec{r}, \nu, z)$	= phase departure of radio waves travelling through the ionosphere
τ	= hour angle
τ_D	= time delay
τ_g	= geometrical time delay difference
$\Upsilon(\gamma)$	= function of γ for the near field corrections (depending on strength of scintillation)
$\chi(\vec{r}, \nu, z)$	= log-amplitude of radio waves travelling through the ionosphere
Ω	= angular velocity due to the Earth's rotation

In section 8 we summarize a method to correct radio interferometric observations for ionospheric refraction. During recent decades a number of authors have estimated ionospheric refraction assuming that the ionosphere is a spherical shell concentric with the Earth (*e.g.*, Belyaev, 1955; Link, 1957 and Chvojkova, 1958a,b). The effects of the spherically symmetric ionosphere and horizontal and vertical gradients in the electron density distribution will be explained.

In section 9 we evaluate ionospheric information that can be derived from measurements with different techniques: *i.e.*, how do these results compare with each other?

Table I lists all symbols used in the text.

2. Observables

A simple two-element interferometer, the building block of all arrays, is shown in fig. 1. Consider a monochromatic signal of frequency ν emanating from a point source whose direction is given by $\vec{r}$. Two elements separated by a fixed baseline $\vec{B}$ intercept the radiation, two samples of which are then transported without loss of characteristics to a common point where they are correlated; *i.e.*, their time averaged sum or product is taken. In most arrays the radio frequency ν is converted to an intermediate frequency (IF) ν_{IF}, by mixing with a common local oscillator signal of frequency ν_0, before transmitting the signals to the central point. The time delay τ_D is usually inserted in the IF line to compensate for the geometric time delay difference τ_g in the arrival of the radiation to each element.

Usually a complex notation is used for the response after correlation. The phase of the response is equal to the *phase* path length difference between the two radiation paths.

The diurnal motion of an extraterrestrial radio source continuously varies the geometric delay causing the response to have a quasi-sinusoidal behavior, so-called fringes. Alternatively, the fringes can be described as a «beating» of the two signals which are Doppler shifted to slightly different frequencies at the correlator due to the relative motion of the two elements with respect to the source.

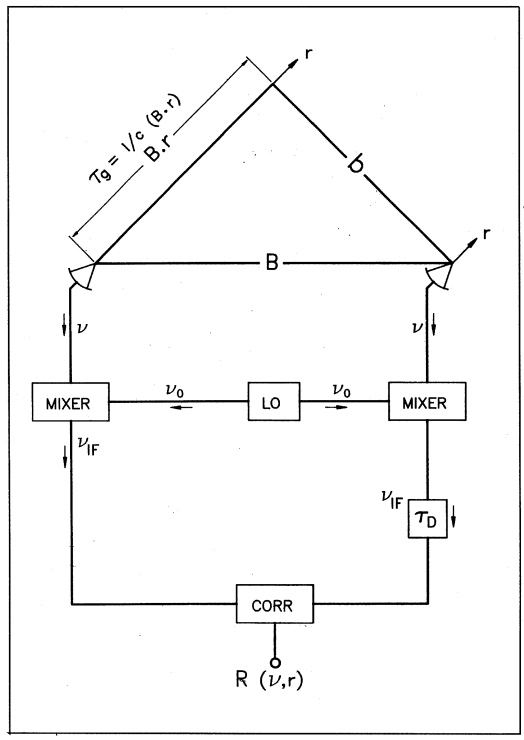

Fig. 1. Schematic diagram of a simple two-element interferometer.

For observations over a larger frequency bandwidth $\Delta\nu$ the differential time delay $\Delta\tau$ between the signals at the correlator point must be smaller than $(\Delta\nu)^{-1}$ to ensure that the entire bandwidth adds in phase. Thus the inserted delay τ_D is usually varied to compensate properly for the change τ_g. Assuming accurate delay tracking with respect to an angular position $\vec{r}_0$, the interferometer response becomes (Thompson, 1989)

$$R(\nu, \vec{r}) = S_\nu \exp\left[j2\pi\frac{\nu_0}{c}\vec{B}\cdot\vec{r}_0\right]\cdot$$

$$\cdot \exp\left[j2\pi\frac{\nu}{c}\vec{B}\cdot(\vec{r}-\vec{r}_0)\right]. \qquad (2.1)$$

The response to an extended source $I(\vec{r}-\vec{r}_0)$ with a wide bandwidth interferometer having a frequency characteristic of $F(\nu)$ and a primary power pattern $G(\vec{r}-\vec{r}_0)$ – *i.e.*, the product of the voltage pattern of each element – is given by integrating (2.1) over $\vec{r}$ and ν

$$R(\nu, \vec{r}) = S_\nu \exp\left[j2\pi\frac{\nu_0}{c}\vec{B}\cdot\vec{r}\right]\int\int F(\nu)\cdot$$

$$\cdot G(\vec{r}-\vec{r}_0) I(\vec{r}-\vec{r}_0)\exp\left[j2\pi\frac{\nu}{c}\vec{B}\cdot(\vec{r}-\vec{r}_0)\right]\mathrm{d}\vec{r}\,\mathrm{d}\nu \equiv$$

$$\equiv S_\nu \exp\left[j2\pi\frac{\nu_0}{c}\vec{B}\cdot\vec{r}_0\right] V(\vec{B}). \qquad (2.2)$$

For simplicity, the angular dependence of the source and the power pattern are assumed to be independent of frequency and normalized at $\vec{r}_0$. The response is composed of two parts: the fast time dependence (fringes) is equal to the response of a point source at $\vec{r}_0$ at an observing frequency ν_0. A slower varying quantity $V(\vec{B})$, the visibility function, describes the amplitude and phase offsets of the fringes (Thompson, 1989). In general, the visibility function is a complicated function of the bandwidth, emission extent, and baseline geometry. The visibility function is closely related to the spatial mutual coherence function used in coherence theory (*e.g.*, Fomalont, 1973). Since in this investigation we deal with point sources only, the following discussion takes eq. (2.1) as its starting point.

3. The Westerbork Synthesis Radio Telescope (WSRT) and its observations

The WSRT is a radio interferometer array described in detail elsewhere (Baars *et al.*, 1973; Högbom and Brouw, 1974; Casse and Muller, 1974; Bos *et al.*, 1981). The instrument is situated at 6.6°E, 52.9°N and consists of 14 steerable paraboloids. Ten occupy fixed positions at 144 m intervals along a 2.7 km east-west baseline: these telescopes are denoted 0, 1, 2, ..., 9. Four additional movable paraboloids (*i.e.*, A, B, C and D) serve as references with respect to which the phase of the radiation received by the antennas 0 to 9 is measured. To this end the latter are connected to the former to form a total of 40 correlation interferometers. The backend of each of these consists of a correlator system which measures the four complex correlations necessary to characterize the polarization state of the radiation. The WSRT has been operating since 1970 in the 21 cm band, since 1973 in the 6 and 49 cm bands, since 1980 in the 18 cm band especially as a node in the European VLBI network, EVN, and since 1983 in the 92 cm band. The observations have been carefully archived since the WSRT became operational.

A source is observed by tracking it in its diurnal rotation from 6 h before to 6 h after meridian transit or over some fraction of this range. The array beam is continuously steered by proper phasing of the elements (*i.e.*, proper delay tracking). This is done with very high precision: positional accuracy in the sky is better than 0.1″, the corresponding phase accuracy better than 1 mm. This precision involves a large number of corrections, both for astrometric effects (Brouw, 1969, 1971; Högbom and Brouw, 1974; Spoelstra, 1983) and for known instrumental errors (Van Someren Gréve, 1974). Point sources with known brightness and position are observed quite frequently for checking and calibrating the instrument. For such sources, we know that the incident wavefront should be perfectly flat; any deviations after application of known astrometric and instrumental corrections must be the result of propagation effects (*e.g.*, Hamaker, 1978; Spoelstra, 1983).

Given the fact that propagation effects are relatively easy to trace in the observed parameters of point sources, this information can also be used as input for studies of the propagation medium (*e.g.*, Spoelstra, 1992a). In particular ionospheric characteristics may be investigated by using these observational data at wavelengths longer than about 20 cm (for the WSRT). These observations have been used for climatological studies of the ionosphere (*e.g.*, Kelder and Spoelstra, 1984; Spoelstra and Kelder, 1984; Van Velthoven, 1990; Spoelstra,

1996). In particular the interferometer phase data are taken for this analysis.

WSRT observations at 21, 49 and 92 cm wavelength from the WSRT archive for the period 1970-1991 have been used as input for the present investigation. For each UT 30 min interval during which an appropriate WSRT observation has been made, the variation in TEC as derived from interferometer phase variations is given in units of number of electrons per m^3,

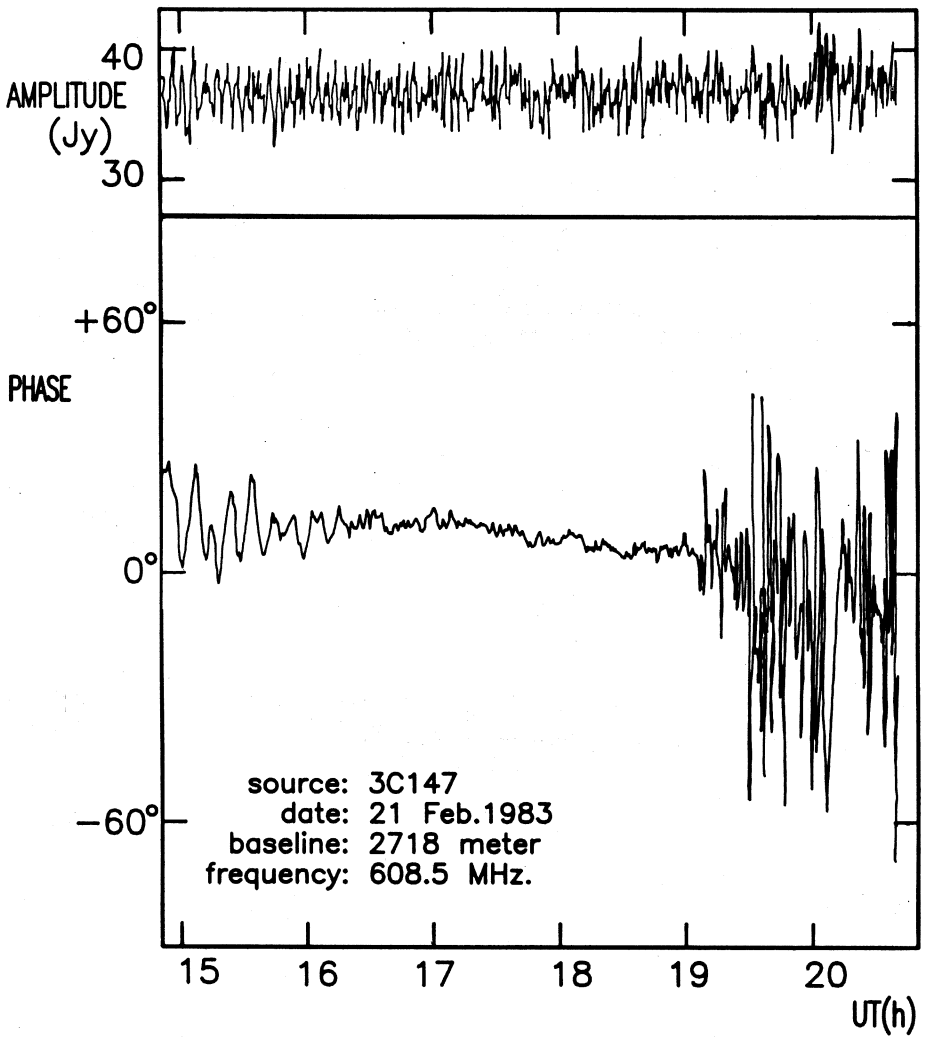

Fig. 2. Ionospheric effects observed with the Westerbork Synthesis Radio Telescope, WSRT. The upper frame shows interferometer amplitude and the lower frame the phase errors. The interferometer baseline is 2.7 km. The ionospheric effects are only seen in interferometer phase. This registration shows slowly varying waves during the first 1.5 h (medium scale TIDs) and rapid variations (phase scintillation) during the last 2.5 h, both superimposed on a slowly varying background (which is due to the daily variation of the electron content).

together with the period of this variation in minutes for manifestations of acoustic gravity waves. In total 38152 half-hour observations have been analyzed. A typical duration of such an observation is of the order of 1 h, while observations of up to 12 h exist in the data base. An example of a registration obtained with the WSRT giving the variation of amplitude and of interferometer phase $\Delta\phi$ as a function of time is given in fig. 2. We know that we are dealing with ionospheric refraction effects since the errors correspond with the calculated values and the frequency dependence of the errors corresponds with what is expected for ionospheric effects. The fluctuations in fig. 2 in $\Delta\phi$ have different time scales: a) a large scale slowly varying «baseline» is caused by the daily variation of the TEC; b) before about 16.30 UT manifestations of medium scale travelling ionospheric disturbances, MSTIDs, are seen; c) after about 19.00 UT the observation is affected by ionospheric scintillation.

4. Propagation effects on measured signals: ionospheric refraction

As the radio wave passes through a refractive medium, this medium modifies the propagation path and the phase of the wave. The ionospheric electron density varies with geographical coordinates and altitude. Therefore, the refractive index will vary in a complicated way along the line of sight (Komesaroff, 1960; Spoelstra, 1983). The wave emerging from this medium has a correlator response of the form

$$R(\nu, \vec{r}) = R_0 \exp [j 2\pi \vec{B} \cdot \vec{r}] \qquad (4.1)$$

where

$$R_0 = S_\nu \exp [j 2\pi (\vec{B}_0 - \vec{B}) \cdot \vec{r}_0]. \qquad (4.2)$$

Then the optical phase path r can be written as

$$r = \int n(\vec{s}, \nu)\, \mathrm{d}s \qquad (4.3)$$

where $n(\vec{s}, \nu)$ is the refractive index of the medium. The integration is performed along the ray path. The range error Δr is

$$\Delta r = \int_\rho n(\vec{s}, \nu)\, \mathrm{d}s - \int_\Sigma \mathrm{d}s_0 = \int_\Sigma (n(\vec{s}, \nu) - 1)\, \mathrm{d}s_0 + \\ + [\int_\rho n(\vec{s}, \nu)\, \mathrm{d}s - \int_\Sigma n(\vec{s}, \nu)\, \mathrm{d}s_0] \qquad (4.4)$$

where $\mathrm{d}s$ is a path element along the ray (ρ indicates integration along the ray path) and $\mathrm{d}s_0$ is a path element along the straight line (the unperturbed ray – Σ indicates integration along the geometrical straight line). The term between brackets on the right hand side of eq. (4.4) is proportional to $(n(\vec{s}, \nu) - 1)^2$ if the refractive index is close to unity everywhere (Weenink, 1987; Van Velthoven, 1990). This condition is fulfilled in the ionosphere and in the troposphere.

Refraction causes a shift, $\Delta\vec{r} = (\vec{r} - \vec{r}_0)$, of the apparent positions of extra-terrestrial objects on the celestial sphere. This shift depends on the geometry of the refractive medium and on the variation of gas or electron density (particularly the gradients along and perpendicular to the line of sight) (Spoelstra, 1983, 1984a).

We can write the eq. (2.1) as

$$R(\nu, \vec{r}) = S_\nu \exp [j 2\pi \vec{B}_0 \cdot \vec{r}_0] \cdot \\ \cdot [\cos (2\pi \vec{B} \cdot \Delta\vec{r}) + j \sin (2\pi \vec{B} \cdot \Delta\vec{r})]. \qquad (4.5)$$

When a point source is observed and the astrometric and instrumental calibration has been performed correctly, the real part of eq. (4.5) expresses the amplitude of the source. The imaginary part of eq. (4.5) gives the interferometer phase error due to refraction effects which is expressed by

$$\Delta\phi = 2\pi \vec{B} \cdot \Delta\vec{r}. \qquad (4.6)$$

Thus the position error causes an error in the phase difference between signals received at the antennas of two elements of an interferometer (*i.e.*, an error in interferometer phase) $\Delta\phi$ at a relative distance of B.

Since in the case of radio interferometry one subtracts the phases of two signals that propagate along almost parallel rays separated by a some distance (from a few kilometres to VLBI

scale), besides the Total Electron Content (TEC) the *gradients* in the ionospheric electron density and the *sphericity* of the atmosphere will play a major role (Spoelstra, 1983, 1987a,b).

Since the presence of the geomagnetic field makes the ionospheric plasma a doubly refractive medium, it will support two orthogonal circularly polarized waves travelling with slightly different phase velocities. The ionosphere affects the state of polarization in the sense that the polarization ellipse is rotated. This is Faraday rotation, which also varies in inverse proportion to the observing frequency squared. Faraday rotation does not depolarize an arbitrary ray – it is manifest in the interferometric amplitudes: i) when the amplitude is expressed in terms of the Stokes parameters; ii) when in *e.g.*, VLBI due to the inhomogeneities in the ionosphere and its geometry, differential Faraday rotation causes different responses for the different interferometer elements.

Both ionospheric refraction and Faraday rotation depend on the columnar electron density along the line of sight. The change in the phase difference due to ionospheric refraction observed by a radio interferometer with elements at $\vec{r}_0$ and $(\vec{r}_0 + \vec{B})$ can be approximated by

$$\Delta\phi = \phi(\vec{r}_0 + \vec{B}) - \phi(\vec{r}_0) \approx \frac{e^2 \vec{B}}{4\pi m_e \varepsilon_0 \nu c} \sec k_0 \nabla N(\vec{r}) \tag{4.7}$$

where m_e is the electron mass, ε_0 is the permittivity of vacuum, e is the electron charge, k_0 is the zenith angle at ionospheric height (assumed value: 350 km) and $N(\vec{r})$ is the electron density distribution. The operator ∇ refers to the horizontal and vertical gradients in the electron distribution. The interferometric phase error at baseline B (in m) due to ionospheric irregularities (*e.g.*, TIDs) can also be approximated by (Hagfors, 1976):

$$\Delta\phi = 84.4 \times 10^8 \frac{kpB}{\nu \cos k_0} \int N(\vec{s}, \nu)\, \mathrm{d}s \tag{4.8}$$

where k is the wavenumber of the density wave, ν is the observing frequency (in Hz), p is the fraction of the total electron content involved in the density waves, N the electron density (in m^{-3}) as a function of position s along the line of sight. When we use S.I. units the Faraday rotation $\Delta\psi$ can be written as

$$\Delta\psi = 2.36 \times 10^4 \nu^{-2} \int N(\vec{s}, \nu) H \cos\theta \, \mathrm{d}s \tag{4.9}$$

where H is the strength of the geomagnetic field (Wb m^{-2}) and θ the angle between the ray and the magnetic field (in radians). Then

$$\frac{\Delta\phi}{\Delta\psi} = 3.6 \times 10^{-11} \frac{\nu k p B}{\cos k_0} \frac{\int N(\vec{s}, \nu)\, \mathrm{d}s}{\int N(\vec{s}, \nu) H \cos\theta \, \mathrm{d}s}. \tag{4.10}$$

If a typical density wavelength is 100 km, $p = 5\%$, $H = 0.5 \times 10^{-4}$ Wb m^{-2}, $\theta = 0$, $z = \pi/4$ the ratio $\Delta\phi/\Delta\psi$ at a baseline of 1 km equals then $3.2 \times 10^{-9}\nu$. In the case of the WSRT at B = 3 km we find that $\Delta\phi/\Delta\psi = 9.6 \times 10^{-9}\nu$. This indicates that at all frequencies larger than about 100 MHz the interferometer phase is more sensitive to ionospheric irregularities than Faraday rotation. This is illustrated in fig. 3, which shows for a WSRT observation of 3C286 at 608.5 MHz (with a degree of polarization of 2.4% at this frequency) and 2.7 km baseline a comparison between $\Delta\phi$ and the polarization angle ψ_{pol} as a function of hour angle. In this case $\Delta\phi$ and ψ_{pol} have not been corrected for ionospheric effects. At this frequency, the instrumental noise of the interferometer phase, $\Delta\phi$, is 0.14°, and of polarization angle, ψ_{pol}, it is 4.2°.

These variations in $\Delta\phi$ may be distinguished in two ways: as «noise», *i.e.* variations for which no clear periodicity above the instrumental noise could be determined, or (generally) as manifestations of acoustic-gravity waves. The latter are often manifestations of travelling ionospheric disturbances, TIDs, of different scales (for which the periods have also been determined) (*e.g.*, Spoelstra and Kelder, 1984; Spoelstra, 1992a). The fluctuations in $\Delta\phi$ obtained after the proper scaling in this way can be converted into variations in the

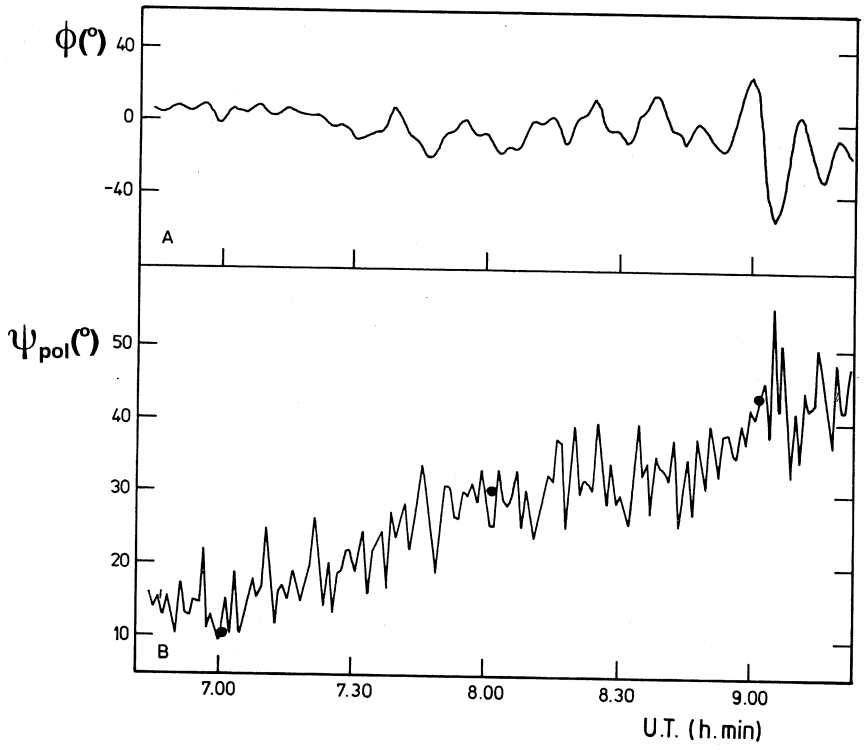

Fig. 3. Variations of phase, ϕ, at 2.7 km baseline and polarization angle, $\psi_{\rm pol}$, for radio source 3C286 observed on January 16, 1982, with the WSRT. Note the different scales for the phase and for the polarization angles. The thick dots in the plot of the polarization angles show the Faraday rotation calculated on the basis of f_0F_2 values observed at the Netherlands Royal Meteorological Institute at De Bilt (with the same zero level as the polarization angles). The f_0F_2 data represent the critical frequencies for the F_2-layer.

east-west gradient of the (vertical) total electron content by

$$\Delta_e = \frac{4\pi m_e \varepsilon_0 c}{e^2} \frac{\nu \cos k_0}{B} \delta(\Delta\phi). \quad (4.11)$$

The interferometer phase in connected element interferometry is sensitive to ionospheric irregularities at wavelengths longer than about 20 cm. At wavelengths shorter than about 50 cm the influence of the troposphere becomes relatively more noticeable because of the difference in frequency dependence of the refractive indices of ionosphere and troposphere. A way to distinguish between both effects in the data has been described by Spoelstra (1996).

5. Climatology of ionospheric irregularities

The calculated variations in the east-west gradient of the vertical total electron content have been correlated with the quiet/disturbed conditions with solar activity, geomagnetic activity, as a function of time of day, season and phase in the solar cycle. It has been assumed that such a comparison is meaningful on the basis of well-known or likely relations of ionospheric parameters with these conditions.

There is no reason to assume that ionospheric effects are related to the civil calender. When we divide the data into intervals of three-monthly seasons, *i.e.* as Winter, Spring, Summer and Autumn, we expect that the re-

sults for Spring and Autumn to be similar. The results for Winter and Summer may differ significantly. The first reason for this is that the declination of the Sun shows this behaviour: it is similar in Spring and Autumn, while it is rather different in Winter and Summer. Spoelstra (1996) analyzed the WSRT-data for a period of 22 years to define the dates for the seasons. Assuming that averaged over all years the Spring and Autumn results should be the same within the errors, he found that this condition is fulfilled when the Winter starts on day 348 ± 3 (+1 day for a leap year) and all seasons last for three months. This implies that the «ionospheric seasons» show no relation with the declination of the Sun or meteorological seasons.

The disturbance of a medium is usually expressed in terms of the frequency of occurrence of the disturbances and the magnitude of these disturbances. As soon as the disturbance has been classified one likes to know *e.g.*, whether it is periodic and what its period is.

5.1. *Occurrence of travelling ionospheric irregularities*

Figure 4 shows the frequency of occurrence of travelling ionospheric disturbances, TIDs, as a function of year and averaged per quarter. Also the averaged R12 sunspot numbers are represented to indicate solar activity. The parameter R12 has been taken as a measure of

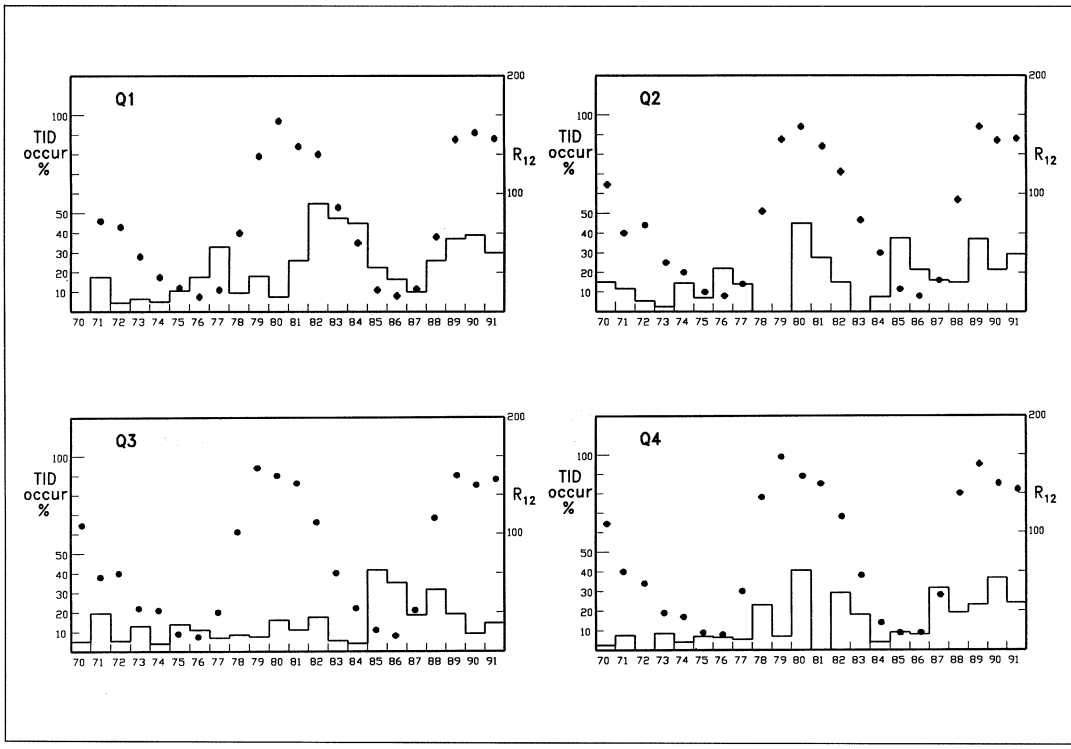

Fig. 4. Frequency of occurrence of medium scale TIDs per quarter as a function of year. The quarters 1 to 4 are indicated by $Q1$, $Q2$, $Q3$ and $Q4$, respectively. The horizontal axis indicates the year. The left hand ordinate gives the frequency of occurrence in %. The right hand ordinate gives the $R12$ sunspot number to indicate the solar activity (the dots represent the values for the different quarters).

solar activity. Figure 4 suggests that the frequency of occurrence of TIDs is different per season. It is obvious from fig. 4 that the frequency of occurrence shows no relation with solar activity. Nor does it show an obvious trend.

Figure 5 shows the frequency of occurrence of travelling ionospheric disturbances as a function of time in the day grouped according to the four quarters of each of the individual 22 years. In the grey scale representation white shows those time intervals for which no data are available. This can be due to the scheduling of the telescope, defective data or too short a duration of the observations.

Figure 5 indicates that in the 1st and 4th quarters the frequency of occurrence of TIDs shows a maximum at noon with a possible minimum before sunrise and sunset, and often a secondary maximum around midnight. It is known from previous work (Spoelstra and Kelder, 1984; Van Velthoven, 1990) and supported by the present data that the noon maximum coincides almost with local noon, which occurs at about 11 h 34 UT. The pattern of the 1st and 4th quarters is much less pronounced during the 2nd and 3rd quarters during which any systematic pattern may even be absent in several years. As in fig. 4 a relation with solar activity expressed by R12 is not clear.

These results obtained by Spoelstra (1996) are basically similar to those which were obtained by Munro (1958), Titheridge (1968), Evans (1983), Waldock and Jones (1986), Kelder and Spoelstra (1984, 1987), Spoelstra and Kelder (1984) and Van Velthoven (1990), although their data bases are up to several orders of magnitude smaller than the one of Spoelstra (1996). Their results were also obtained at other places by a wide range of techniques. The observed daily variation in the frequency of occurrence of TIDs ought to be compared with the daily variation in the visibility of TIDs. During night time the visibility is expected to be smaller because the night time electron density is smaller than the daytime one, which is in contradiction with the observed large night time frequency of occurrence of TIDs.

Van Velthoven (1990) showed that there is a significant difference of the frequency of oc-

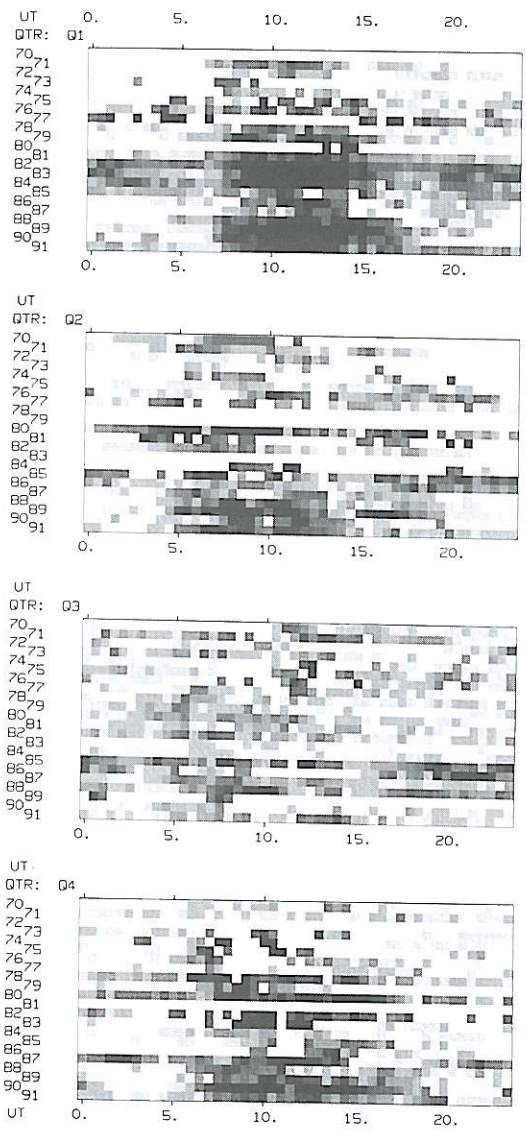

Fig. 5. Frequency of occurrence of medium scale TIDs as a function of time in the day per quarter as a function of year. The quarters 1 to 4 are indicated by *Q*1, *Q*2, *Q*3 and *Q*4, respectively. The horizontal axis indicates the time in UT hours. The ordinate indicate the year. The frequency of occurrence in %: the values are expressed by grey scale levels. The grey levels intervals are: 0-10, 10-20, 20-30, 30-40, 40-50, 50-60, 60-70 and > 80% (= dark). White indicates that there are not enough data for that bin.

currence of TIDs with the direction of the line-of-sight. Relatively minor differences are found between eastward and westward lines-of-sight. Somewhat more are observed with an eastward line-of-sight around noon. For northward directions of the line-of-sight the distribution is similar but more irregular and perhaps somewhat broader. For southward directions the difference is dramatic: hardly any variation with time is seen and the frequency of occurrence is low (about 25%). Van Velthoven (1990) explains this phenomenon as due to variation of the angle of the line-of-sight with the TID wave vector in relation to the sensitivity of the WSRT for gradients in the ionospheric electron distribution as a function of direction. The best visibility is reached when one looks along the planes of constant phase of the TID. The planes of constant phase of upward propagating TIDs are tilted forward, so the largest response is found if the *horizontal* components of the line-of-sight vector and the wave vector are almost parallel. This means that *e.g.*, eastward propagating TIDs are best visible with an eastward line-of-sight. The fact that the frequency of occurrence with eastward lines-of-sight is larger than with westward lines-of-sight around noon would then imply that around noon more TIDs have phase velocities with an eastward component rather than with a westward component. This has been observed by Waldock and Jones (1986) and Kalikhman (1980).

5.2. *Amplitude of medium scale TIDs*

The daily variation in the amplitude of medium scale TIDs exhibits a mainly semidiurnal variation with maxima around noon and midnight. The noon maximum occurs slightly before 12 h UT: in fact it coincides almost with local noon, which occurs at about 11 h 34 UT.

The frequency of occurrence of TIDs and the amplitude of TIDs show similar daily and seasonal variations. This is related to the fact that TIDs with large amplitudes are better visible than those with small amplitudes.

The daily variation of the TID amplitude as a function of season for the different years is given in fig. 6. The open boxes show the values for 49 and 92 cm data (including bars indicating the mean errors), while the filled boxes show the values from all data.

Figure 6 shows that during the Winter season the pattern of the variations of the mean amplitudes as a function of time in the day is symmetric around local noon. A similar result has been obtained in previous analyses by *e.g.*, Kelder and Spoelstra (1984, 1987), Van Velthoven (1990), Mercier (1996) and Spoelstra (1996). When the Sun is below the horizon significant irregularities are still observed. Kelder and Spoelstra (1987) observed that the amplitude of TIDs oscillated with 24, 12 or 8 h periods from a Fourier decomposition of the variations of the mean amplitudes as a function of time in the day. Oscillations of atmospheric variables with 24, 12 or 8 h periods are manifest for upper atmospheric tides (Chapman and Lindzen, 1970). These tides may play a role in the generation of gravity waves. Experimental evidence of a relation between the intensity of internal gravity waves and tides has already been presented by Gavrilov *et al.* (1981) and also found by Canziani (1994) and Fritts and Vincent (1987). These tidal waves excited in the lower atmosphere (*i.e.*, the stratosphere and troposphere) grow with height h as $\exp(h/2H)$, where H is the scale height of the atmosphere. Between 80 and 120 km altitude they can reach amplitudes of the order of 150 m/s^{-1}. At this height they travel through the temperature minimum of the atmosphere. This means that we have low values of the Brunt-Väisälä frequency and that the Richardson number corresponding with the tidal velocity field is small. Thus, tidal waves become unstable and can generate internal gravity waves. Their horizontal phase speeds have to correspond to the amplitude of the tidal waves (Drazin and Reid, 1981). That horizontal speeds of this order are common for the wavelike phenomena discussed in this paper has been shown by Spoelstra (1992b).

The results of the Fourier decomposition of the mean TID amplitudes from the Winter data is given in table II. Clearly dominant are the 12 h and 8 h period components. High order terms

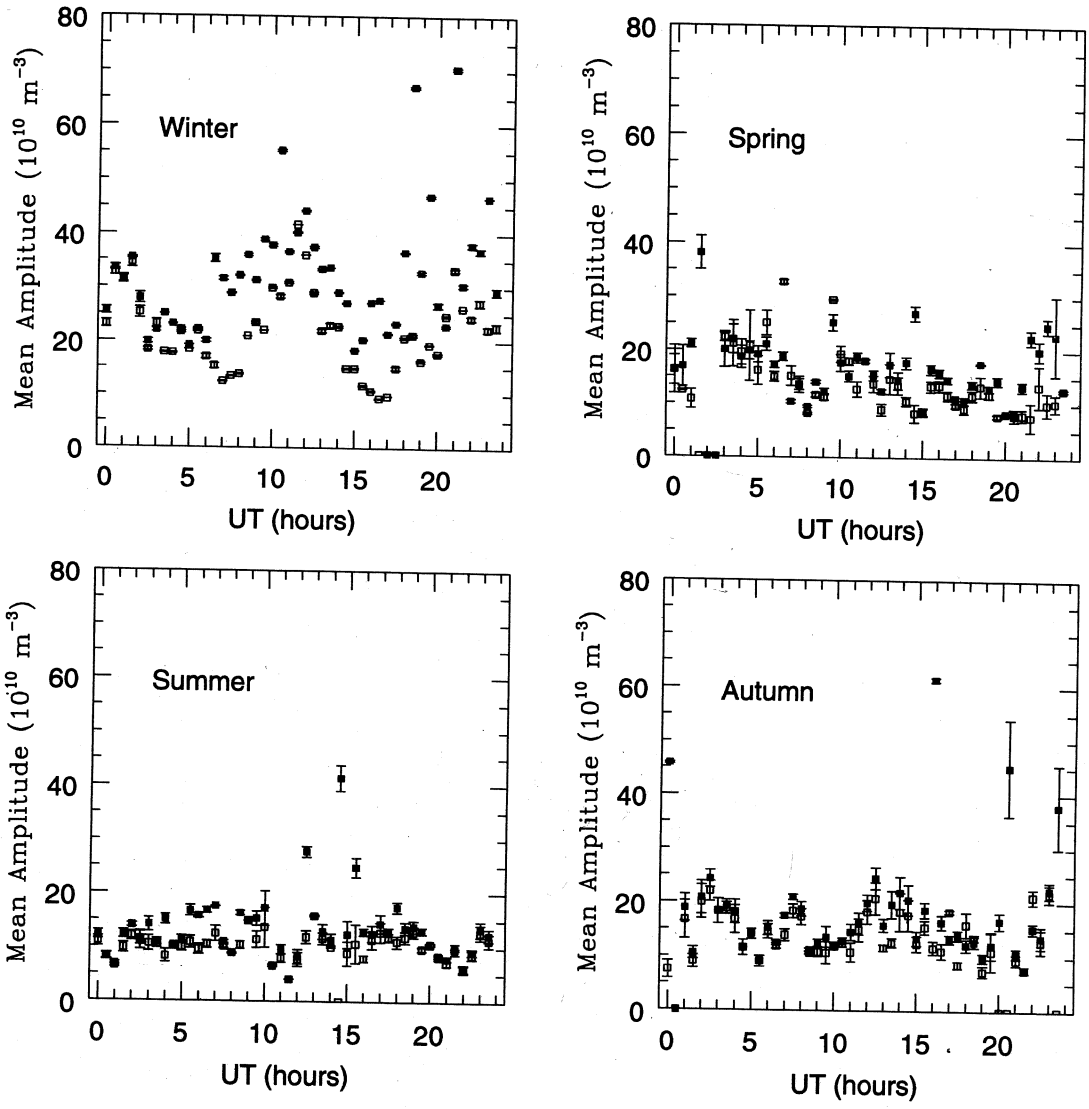

Fig. 6. The averaged mean amplitude for the different years in TEC units of $10^{10}m^{-3}$. The open boxes represent the values for 49 and 92 cm data (including bars indicating the mean errors), while the filled boxes show the values from all data.

are less significant. Figure 6 also shows the results for the other seasons which have larger standard deviations than the Winter data. The Summer data show no significant variation of TID amplitudes with time, while during Spring and Autumn the 24 h, 12 h and 8 h periods may be significant. This does not imply that such periodicities do not exist in Summer, but they may be out of phase to such an extent that their effect cancels. There is a slight tendency

Table II. Fourier decomposition mean TID amplitudes. The mean TID amplitude, A, is given in units of 10^{10} m^{-3}; the phase offset, Φ, taken from the meridian is given in °; P gives the Fourier components.

Season	Zero-level	P = 24 h		P = 12 h		P = 8 h		Averaged A
	A	A	Φ	A	Φ	A	Φ	
Winter	21.9	1.5	239.2	7.6	179.5	4.0	3.5	
	± 0.4	± 0.2	± 6.0	± 0.2	± 3.4	± 0.2	± 5.9	
Spring	15.9	7.3	258.5	4.3	278.1	4.4	313.0	17.2
	± 0.2	± 0.1	± 1.5	± 0.1	± 3.6	± 0.1	± 4.5	± 0.3
Summer	10.2	0.3	16.9	0.7	1.4	0.6	243.1	10.2
	± 0.2	± 0.1	± 26.6	± 0.1	± 19.1	± 0.1	± 9.9	± 0.2
Autumn	14.9	1.4	158.8	0.3	196.1	2.1	46.7	13.0
	± 0.2	± 0.1	+ 14.6	± 0.2	± 37.6	± 0.2	± 0.3	± 0.6

for the amplitudes to be somewhat larger in Spring than in Autumn. Because of the difference with the Winter results table II also gives the averaged values for the other seasons.

The pattern observed for the Winter season differs from that in other seasons. We note that particularly Winter data (see also *e.g.*, Fritts and Vincent, 1987) suggest a relation between internal gravity waves and tides. Its seasonal dependence is subject to further investigations.

If the disturbance of the ionosphere shows a systematic dependence on time of day, season, solar activity, this does not automatically imply that there are no significant deviations from this dependency. But since the mean errors on the mean TID amplitudes show no obvious dependence on time or season we conclude that there exist no periods when intrinsically the disturbance of the ionosphere is less well determined than in other periods (Spoelstra, 1996). We note that *e.g.*, due to the relatively rapid increase in the degree of ionization and changing of the vertical electron distribution during sunrise hours such an erratic behaviour might not be unexpected. But this is not found.

5.3. *Classification of the disturbances*

The averaged mean period of TIDs for the different seasons is represented in fig. 7. Especially in the Winter months this behaviour is clear: the periods are longer in daytime than during the night. The results of a Fourier analysis of these data are given in table III. In several years and seasons the night time values of the period are smaller than the daytime ones (*e.g.*, like the Winter of 1983-1985). Furthermore, the daily variation is somewhat more pronounced in Winter than in Spring/Autumn. The average TID period is largest for the Spring and Summer seasons than for the other seasons. We also note the existence of a relative minimum around noon in all seasons.

The periods exhibit values typical for medium scale TIDs and are consistent with the Brunt-Väisälä period. Larger scale TIDs were not usually detected. This is not due to a selection effect deriving from the limited duration of observations in the WSRT data base (which can be up to 12 h). But the sensitivity of the WSRT to large scale TIDs which propagate presumably away from the auroral region is rather low since this instrument is an east-west array.

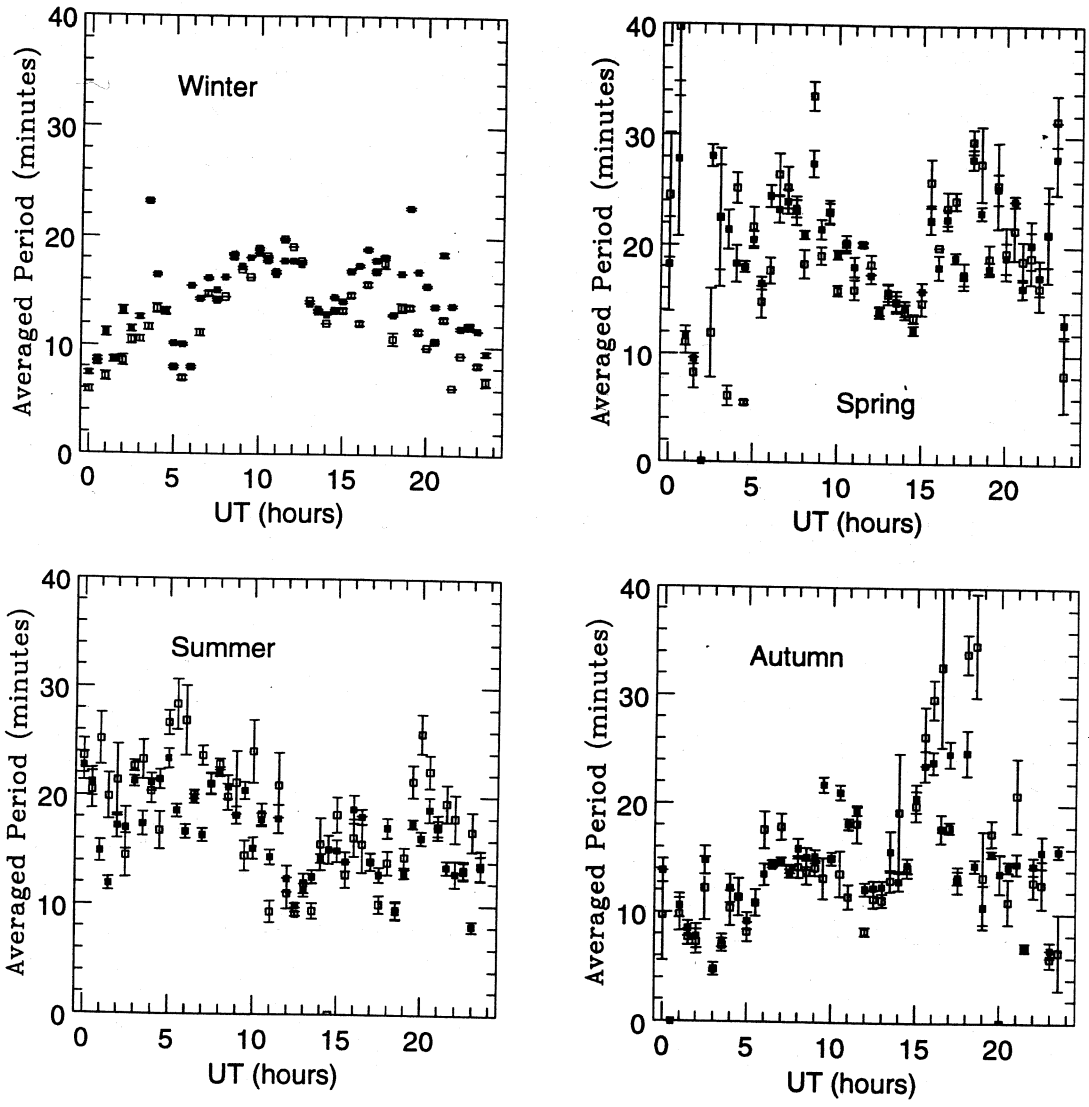

Fig. 7. The averaged mean period of TIDs for the different years. The open boxes represent the values for 49 and 92 cm data (including bars indicating the mean errors), while the filled boxes show the values from all data.

The variations in the TID periods can, however, not be explained by variations in the Brunt-Väisälä period due to thermal tides in the ionosphere (Alcayde, 1974; Van Velthoven, 1990).

If the daily variation in the period of TIDs is partly due to Doppler shifting or filtering of acoustic-gravity waves by tidal winds, different daily variations should be observed for different directions of the line of sight. This effect was indeed observed by Van Velthoven (1990) using a representative subset of the present data base. The usually relatively small night time values of the TID period may be ex-

Table III. Fourier decomposition mean TID periods. The mean TID period, Π, is given in minutes; the phase offset, Φ, taken from the meridian is given in °; *P* gives the Fourier components.

Season	Zero-level	*P* = 24 h		*P* = 12 h		*P* = 8 h		Averaged Π
	Π	Π	Φ	Π	Φ	Π	Φ	
Winter	12.6	4.2	12.5	0.8	104.9	1.7	310.0	
	± 0.1	± 0.1	± 1.3	± 0.1	± 11.1	± 0.0	± 6.0	
Spring	19.5	1.3	96.8	3.8	74.2	2.8	217.6	15.1
	± 0.2	± 0.1	± 7.6	± 0.1	± 1.6	± 0.1	± 0.6	± 10.5
Summer	18.2	4.4	247.5	1.9	46.4	0.7	135.4	14.6
	± 0.2	± 0.2	± 1.9	± 0.1	± 0.3	± 0.1	± 30.5	± 0.6
Autumn	15.3	5.5	80.0	3.7	15.9	2.9	236.4	12.3
	± 0.1	± 0.1	± 1.0	± 0.1	± 1.2	± 0.1	± 0.6	± 0.5

plained by assuming that on average the meridional component of the wave vector of TIDs is southward. Most observers find that during daytime the meridional component of the phase velocity is southward rather than northward, while during night time the observed directions of the phase velocity are somewhat more dispersed (Waldock and Jones, 1986; Kalikhman, 1980; Kelder and Spoelstra, 1987; Mercier *et al.*, 1989; Spoelstra, 1992a; Van Velthoven, 1990). Doppler shifting or filtering will then reduce the average period during night time and increase the average period during day time. This is due to the fact that waves with phase velocities in the direction of and smaller than the background wind will be removed from the spectrum by critical coupling to the background flow, and some of the waves with phase velocities in the opposite direction will be removed from the spectrum by reflection. Waves with phase velocities perpendicular to the direction of the neutral wind are not affected by it. Waves with large periods have in general smaller horizontal phase velocities than waves with small periods (for fixed horizontal wavelength) and will therefore more easily be filtered by critical coupling. So critical coupling will lead to a reduction in the average observed period of acoustic gravity waves that propagate in the horizontal direction of the neutral wind. Acoustic gravity waves propagating away from the observer are best visible, so we expect a reduction of the average observed period if the observer is looking in the direction of the neutral wind. On the other hand, waves with small periods are more easily reflected by the neutral wind than waves with large periods having the same horizontal wavelength. Reflection will lead to an increase in the average period of acoustic gravity waves that propagate in the horizontal direction opposite to that of the neutral wind, so we expect an increase in the average observed period if the observer is looking in that direction.

Thus the action of the neutral wind may be able to explain observed features of the daily variation in the period of TIDs. However, from the available data it cannot be decided whether this action consists of Doppler shifting or filtering.

5.3.1. Propagation parameters of medium scale TIDs

Spoelstra (1992b) derived from simultaneous measurements with the WSRT and of dif-

ferential Doppler shifts observed using NNSS satellites information about the same physical TID wave packet if the lines of sight from the different stations pass through the same region of the ionosphere. His method used the geometrical fact that the WSRT have been built along an east-west baseline and that the NNSS move along polar orbits.

About 30 coincidences (which satisfy the criterion that the lines of sight towards the celestial source and the satellite pass the same region of the ionosphere) during the first three months of 1982 and 1983 were selected. The calculated azimuth and speed of propagation for these waves are represented in fig. 8. A histogram of the computed distances between the ridges is given in fig. 9. An altitude of 400 km for the calculation of the speed has been assumed.

These results indicate that most of the medium scale TIDs which have been analyzed propagate roughly north > south, with a devia-

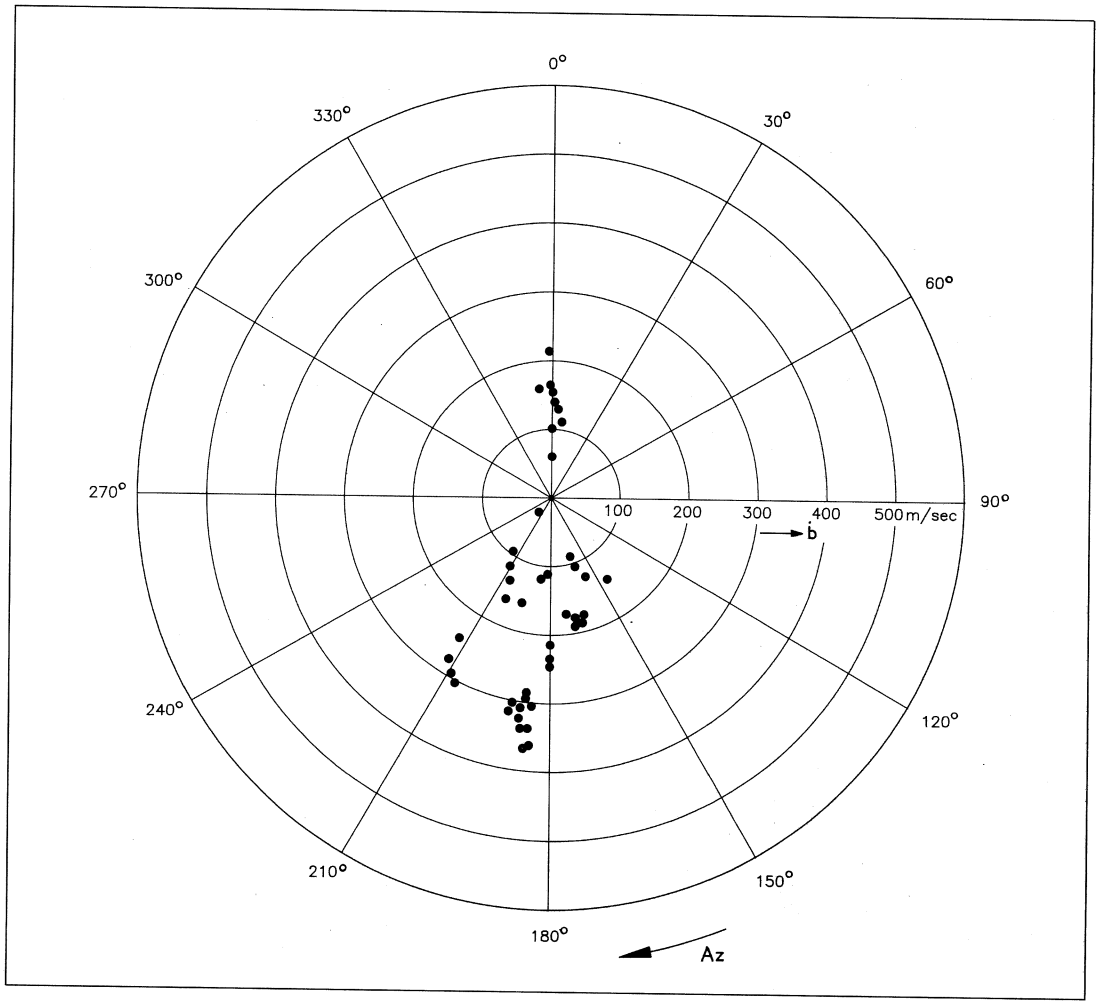

Fig. 8. Distribution of azimuths, Az, and speeds, $\dot{b}$, of 30 TID events in 1982 and 1983.

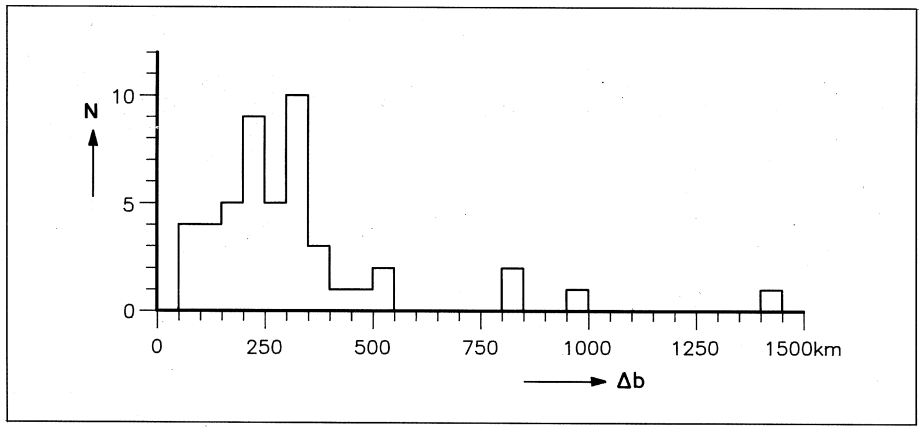

Fig. 9. Histogram of the horizontal linear dimensions, Δb, of the analyzed TIDs.

tion of about 10° to the west. Often for one TID-«train», the calculated azimuth and speed of propagation for these waves, their period and the distance between the ridges (or «wavelength») for the different ridges are different from each other. Although this is not unexpected, it indicates that the TID-manifestations we observe may be the result of interference between individual waves.

Mercier (1986) used observations with the two dimensional Nançay Radioheliograph done during the same period as mentioned above. He found a dominant azimuth in the south-east quadrant. However the subionospheric coordinates of his observations are of the order of 600 km south of those discussed by Spoelstra (1992b). Thus different parts of the ionosphere were studied.

Van Velthoven *et al.* (1990) found when using observations with the Nancay Radioheliograph and differential Doppler measurements of NNSS satellites a direction of propagation towards about 13° east of south. However, their observing sites are about 800 km south of the WSRT, which is larger than the typical «wavelength» of medium scale TIDs (fig. 9). Furthermore, the observations of Van Velthoven *et al.* (1990) were done more than 4 years after the observations analyzed by Spoelstra (1992b) and Mercier (1986). Therefore, there is not necessarily a significant conflict between the results of these two studies. The complexity of interference patterns between individual wave «trains» may, however, imply that these parameters may vary significantly with geographic coordinates and time.

5.4. *Conclusion on the climatology of ionospheric irregularities*

In conclusion, the analysis of the data base of WSRT observations of ionospheric irregularities has led to the following results:

– The previously found daily variation in the amplitude of TIDs during the first quarter of the year (for 1982 and 1983 as discussed by Kelder and Spoelstra, 1984, 1987 and Spoelstra and Kelder, 1984) has been found to occur also in other years, especially during the Winter (which starts on day 348 ± 3). It does not occur in Summer, however, and it is less pronounced in Spring and Autumn than in Winter.

The daytime variation with its maximum around local noon probably may have to be explained by the variation in the electron density. The observed secondary night time maximum may be due to the irregular night time distribution of the electron density or to an actual

night time maximum in the amplitude of acoustic gravity waves at thermospheric heights.

– The average period of the TIDs reached a maximum during daytime in Winter, a minimum during night time, and was found to depend upon the direction of the line-of-sight (Van Velthoven, 1990). These effects can be explained by the changes in the mean period of acoustic gravity waves caused by filtering or Doppler shifting by the neutral wind.

– There is a variation with season in the frequency of occurrence and the amplitude of TIDs. A broad maximum occurs in Winter, and a minimum occurs in Summer. It is not clear whether a superimposed semiannual variation exists.

– None of the observed TID related quantities showed a significant correlation with any geomagnetic activity indices considered in the analysis (AE-index, a-indices).

– There appears to be no relationship between the amplitude or the frequency of occurrence of TIDs and the solar cycle.

– The thermospheric Brunt-Väisälä period has a solar cycle variation due to its dependence upon thermospheric temperature. No corresponding variation of the period of TIDs was observed.

– The present results do not support the idea that the solar terminator might be an agent to excite ionospheric irregularities. The solar terminator, passing twice each day, would cause a semidiurnal variation in the frequency of occurrence and in the amplitude of the acoustic gravity waves that are generated by it, with the maximum occurring just after sunrise and sunset at ionospheric heights. The temporal variations we observe in our data set do not show such enhancements and we conclude that it is very unlikely that the terminator is an active agent in this context.

The daily variation in the amplitude and frequency of occurrence of the TIDs suggests that the solar terminator and Joule heating near the electrojets do not contribute substantially to their generation. Also the influence of solar activity can be ruled out. A coordinated investigation of TIDs and winds and tides in the lower thermosphere/mesosphere may be worthwhile, with the purpose of investigating further the effects of filtering, Doppler shifting and secondary wave generation upon the acoustic gravity wave spectrum that propagates upward to thermospheric heights (Van Velthoven, 1990).

6. Scintillation

There is a smooth transition from refraction into diffraction. Diffraction occurs when the angular scale of ionospheric irregularities is less than the beamwidth of the instrument: in the case of an interferometer this is the synthesized beam. Diffraction is visible in the observations as scintillations in amplitude. Scintillation in phase is *e.g.*, observed in interferometric observations when small scale ionospheric irregularities cause phase differences in the signals received between the different interferometer elements. Whether these scintillations degrade the observations depends of course on the integration time used and on the primary beam of the instrument. If phase scintillations occur within one integration time the interferometer amplitude is distorted due to decorrelation within the receiver. In radio interferometric observations the scintillation index depends strongly on the distance between the interferometer elements (Spoelstra and Yang, 1995).

6.1. *Observing weak scintillation*

Scintillation is most strongly observed for point sources. In general, the interferometer response for a celestial radio source with flux S_ν in the direction $\vec{r}_0$ can be written as (from eq. (2.2)):

$$R(\nu, \vec{r}) = S_\nu \int \exp\left[j 2\pi \frac{\nu_0}{c} \vec{B} \cdot \vec{r}_0\right] \int\int F(\nu) \cdot$$

$$\cdot G(\vec{r} - \vec{r}_0) \exp\left[j 2\pi \frac{\nu}{c} \vec{B} \cdot (\vec{r} - \vec{r}_0)\right] \mathrm{d}\vec{r}\ \mathrm{d}\nu \mathrm{d}t \quad (6.1)$$

where integration of the time t means integration over the integration time.